"The final publication is available at link.springer.com: https://link.springer.com/article/10.1007%2Fs11095-018-2449-7 "
Acknowledgement to Springer US, DOI: https://doi.org/10.1007/s11095-018-2449-7

Effect of tumor relevant acidic environment in the interaction of a *N*-hydroxyindole-2-carboxylic derivative with the phospholipid bilayer

Daniela Monti, Silvia Tampucci, Erica Zucchetti, Carlotta Granchi, Filippo Minutolo, Anna Maria Piras*

Department of Pharmacy, University of Pisa, Via Bonanno 33 56126 Pisa, Italy

*corresponding author: Anna Maria Piras, anna.piras@unipi.it, +39 0502219704

RUNNING HEAD: antitumor *N*-hydroxyindole derivative and DPPC vesicles

ABSTRACT

Purpose

The inhibitors of the human isoform 5 of lactate dehydrogenase (*h*LDH5) have attracted growing interest as efficient anti-cancer agents. In the present paper, the interactions between an efficient *h*LDH5 inhibitor (*N*-hydroxyindole-2-carboxylic derivative) and lipid bilayers based on dipalmitoylphosphatidylcholine (DPPC) were investigated. Additionally, since interstitial acidification plays a key role in tumor pathogenesis and tumor drug therapy, the effect of acidic pH was assessed and correlated to DPPC/drug interaction.

Methods

Four different techniques were used: differential scanning calorimetry, dynamic light scattering, UV-VIS second derivative spectrometry and attenuated total reflection Fourier transformed infrared spectroscopy.

Results

All techniques concur in highlighting a structural change of lipid assembly, susceptible both to pH change and to the presence of the antitumor compound. Lipid vesicles appeared more compact at the lower pH, since the thermal pre-transition from the lamellar gel phase to the ripple gel phase was

absent at pH 7.4 and the infrared analysis revealed a stronger acyl chain packing as well as a different hydration degree. Drug interaction was mainly detected in the lipid region including the ester linkages and the first portion of the acyl chains. Furthermore, a lower drug partitioning was recorded at pH6.6.

Conclusions

The investigated antitumor agent possesses a stable negative charge at the investigated pH values, thus the lower interaction at the acidic pH is mainly ascribable to an environmental effect on lipid assembly. Therefore, drug efficacy under tumor acid conditions may be hampered by the observed lipid membrane constraints, and suggest for the development of suitable prodrugs.

KEYWORDS

dipalmitoylphosphatidylcholine (DPPC)

N-hydroxyindole derivatives

*h*LDH5 inhibitor

tumor acidic pH

List of Abbreviations

human isoform 5 of lactate dehydrogenase (*h*LDH5)

1,2-dipalmitoyl-sn-glycero-3-phosphocholine (DPPC)

1-Hydroxy-6-phenyl-4-(trifluoromethyl)-1Hindol-2-carboxylic acid (F21)

Differential scanning calorimetry (DSC)

Dynamic light scattering (DLS)

Attenuated total reflection Fourier transformed infrared spectroscopy (ATR-FTIR)

Phospholipids (PL)

Cholesterol (Chol)

Introduction

Solid tumor tissues are characterized by acidic extracellular pH (pHe) ranging between 6.5-6.9, but intracellular ordinary neutral to alkaline pH (pHi) [1]. This interstitial acidification results from several factors, including altered cellular buffering and metabolism systems, as well as defective tissue perfusion. Acidosis has a fundamental role in tumor pathogenesis and progression, but the acidic environment can also limit the effect of therapeutic molecules [2]. Passive diffusion of small molecules through membrane lipid bilayers is a common way to permeate the cells and gain access to intracellular therapeutic targets. It is generally assumed that low molecular weight molecules with high lipophilicity at neutral pH are highly permeable thanks to good partitioning within the bilayers. For tumor tissues, the pHe-pHi gradient is responsible for "ion trapping" (or drug pH partitioning). This process regards the partitioning of pH sensitive molecules on the membrane side where the molecule net-charge precludes or limit the interaction with the hydrophobic bilayer. Ion trapping has been described and well documented for weak acids and weak bases. The net charge of both types of molecules is greatly affected by the relatively small change of pH (from 6.5 to 7.4 of pHe and pHi, respectively). As example, doxorubicin (pK_a 8.3) accesses to the intracellular compartment is hampered by ion trapping, whereas chlorambucil (pK_a 5.8) intracellular fraction is increased by extracellular acidosis. According to this behaviour, and in order to take advantage of tumor acidosis, the use of weak acids is a typical approach for the design of antitumor drugs. Additionally, from this viewpoint, the extracellular acidosis is not affecting the permeability of stronger acids [2], whereas weak bases are trapped on the wrong side of the cellular membranes. Such effect ends up as drug resistance due to extracellular acidosis.

Overall, this picture does not take into account the membrane issue: a possible structural alteration of the membrane bilayer due to small pH changes could affect the interaction of drug molecules carrying stable negative (strong acid) net charges. Indeed, drug interactions with barriers are complex phenomena. These interactions include both polar and hydrophobic aspects. Phospholipids (PL) are

the major components of all cell membranes [3] and can spontaneously self-assemble into lipid bilayers, thanks to their amphiphilic features. The structure of the phospholipid molecule generally consists of two hydrophobic fatty acid "tails" and a hydrophilic phosphate "head", joined together by a glycerol molecule. Phospholipids and, in particular dipalmitoylphosphatidylcholine (DPPC) are commonly adopted as simplified models of biological membranes [4]. DPPC, also known as lecithin, is one of the most representative membrane phospholipids both in physiological and tumor conditions. The main advantage of phospholipid vesicle-like models is their anisotropicity, which allows the occurrence of three-dimensional phenomena between drugs and barriers [5].

In the present study, the interaction between the phospholipid bilayer and the progenitor of a new class of antitumor drugs was assessed both at physiological (pH 7.4) and at interstitial acidic (pH 6.6) conditions, in order to highlight the contribution of the drug-membrane affinity to the antitumor activity. The *N*-hydroxyindole derivative F21 (Structure 1) was developed in 2011 as an anti-cancer agent, which proved to efficiently inhibit the human isoform 5 of lactate dehydrogenase (*h*LDH5) [6]. This enzyme, which catalyses the conversion of the end product of glycolysis (pyruvate) to lactate, plays a key role in the metabolic adaption of cancer cells to the hostile hypoxic micro-environment, allowing their proliferation and survival in conditions of low oxygen concentrations. In the last decade, a growing number of *h*LDH5 inhibitors were developed with the aim of killing cancer cells by starvation, without interfering with the oxidative metabolism of healthy tissues. Compound F21 efficiently inhibited *h*LDH5 in biochemical assays, being competitive with both the cofactor NADH and the substrate pyruvate, and it showed IC_{50} values in the low micromolar range, together with a good degree of selectivity for isoform 5 over isoform 1 [7]. The mechanism of action of this inhibitor was further confirmed by *in vitro* cell-based studies, where it proved to be able to reduce lactate production in HeLa cancer cells and to block cancer cell proliferation, especially under hypoxic conditions [8, 9].

The ionization degree of F21 is not significantly affected by the small pH variation occurring at the

tumor interstitial level, meaning that it does not take any advantage of the ion trapping effect. Thus, the elucidation of the interaction of F21 with DPPC bilayers at physiological and tumor acidic pH values appears helpful for improving the design and future development of new *N*-hydroxyindole derivatives.

DPPC vesicles containing F21 were prepared by reverse-phase evaporation method under two different pHs, representing normal physiological pH (pH 7.4) and tumor interstitial acidic pH (pH 6.6), respectively. In order to assess the interaction between F21 and phospholipid membranes, the prepared vesicles were characterized by means of several complementary techniques, namely differential scanning calorimetry, dynamic light scattering, UV-VIS second derivative spectrometry and attenuated total reflection Fourier transformed infrared spectroscopy.

Materials and Methods

Chemicals

DPPC (1,2-dipalmitoyl-sn-glycero-3-phosphocholine) was purchased from Avanti Polar Lipids. 1-Hydroxy-6-phenyl-4-(trifluoromethyl)-1-hindol-2-carboxylic acid (F21) was synthesized in house as described previously [6]. All other chemicals were of analytical grade.

Vesicles preparation

Vesicles were prepared using REVs (Reverse-phase evaporation vesicles) method [10]. Appropriate amounts of DPPC and F21 were first dissolved in chloroform and ethanol, respectively. Binary mixtures of DPPC and F21 were prepared under the following F21/DPPC molar ratio: 0.06 (DPPC-X1) and 0.13 (DPPC-X2). Following the same experimental procedure, vesicles without drug (empty vesicles, DPPC-E) were prepared. Afterwards, 66.5 mM phosphate buffer solution (PB), either pH 7.4 or 6.6 was added and the organic solvents were evaporated by using a rotary evaporator, under

reduced pressure at 45 °C. The obtained vesicular suspensions were vortex mixed, and sonicated for 5 minutes (ultrasound frequency: 45 kHz; Sonica Ultrasonic Cleaner mod. 2200 ETH, SOLTEC). Lipid final concentration was 34mM for all prepared suspensions.

Differential scanning calorimetry (DSC) studies

DSC measurements were performed using a Perkin Elmer Pyris DSC6 instrument on 30 μL samples of each vesicular suspension, transferred to a 50 μL aluminium pan. Endothermic curves were obtained under a heating rate of 2 °C/min between the temperature range 25-50 °C, after 5 min equilibration at 25 °C. Each vesicular suspension was analysed in triplicate.

Dynamic light scattering (DLS) evaluation

Diameter distribution of the vesicles was evaluated by using Coulter N4 PLUS (Coulter Corporation). 20 μL of samples were added to 2 mL of PB (either at pH 7.4 or 6.6) and analysed at 20 °C. Results are reported as unimodal distribution based on cumulants fitting.

Attenuated total reflection Fourier transformed infrared spectroscopy (ATR-FTIR)

ATR/FT-IR spectra were recorded by using a Cary 660 series Agilent Technologies, between 650 e 4000 cm^{-1}, at 25 °C, 64 scans. The spectra were collected on the vesicular suspensions and plain medium (PB) was used as blank for spectral subtraction. At least, five spectra were collected for each sample.

The spectra were processed by using IGOR PRO 6.05 (Wave metrics). Binomial smoothing (18) was performed and peak positions were assessed from spectrum 2^{nd} derivatives. Spectral deconvolution was performed as Gaussian shape by means of multipeak fitting package and the obtained peaks were used for the evaluation of relative intensity changes.

UV-VIS second derivative spectrometry

The partition coefficients (Kp) of F21 into DPPC vesicles at pH 7.4 and pH 6.6 were determined by second derivative spectrometry, according to Omran A, 2013 [11]. For each assayed conditions, pH7.4 PB and pH 6.6 PB, sixteen 5 mL volumetric flasks were prepared and equally divided into two sets.

One set was used as sample solutions and the other set as reference solutions. The flasks in both sets contained increasing amounts of DPPC vesicles (0-816μM) prepared at the assayed pHs. For the sample's set, F21 was added to each flask to obtain a final concentration of 0.002mg/ml (6.2μM). Each flask was incubated at 40°C for 30 min and then at room temperature (25°C) for 30 min, before performing the spectrophotometric analysis in the 200-400 nm range (Shimadzu UV-2101 PC spectrophotometer, Shimadzu). The absorption spectrum of each sample solution was recorded against the correspondent F21- free sample as reference.

Kp is defined as:

$$Kp = \frac{mol\ of\ F21\ in\ DPPC\ vesicles/mol\ of\ DPPC}{mol\ of F21\ in\ aqueous\ phase\ /water\ mol} \quad (1)$$

and was calculated from the analysis of the second derivative spectra according to

$$\Delta D = \frac{\Delta Dmax\ Kp\ [DPPC]}{[W]+Kp[DPPC]} \quad (2)$$

where ΔD is the difference between the second derivative intensity of sample and plain F21 solutions at predefined wavelengths, ΔDmax is the theoretical higher ΔD value achievable when F21 is totally partitioned into vesicles, [DPPC] and [W] are molar concentrations of lipid vesicles and water (55.34 mol/L at 25°C), respectively. Kp and ΔDmax were calculated by applying the Levenberg□Marquardt algorithm as non-linear least squares fitting method to Eq. (2). The initial values of Kp and ΔDmax were obtained from the Scott-plot method in which Eq. (2) is linearized:

$$\frac{[DPPC]}{\Delta D} = \frac{1}{\Delta Dmax}[DPPC] + \frac{Kp\ [W]}{\Delta Dmax} \quad (3)$$

The spectra were processed by using IGOR PRO 6.05 (Wave metrics). Savitzky–Golay (35) smoothing was performed on absorbance spectra before elaborating the 2nd derivative spectra by central differences algorithm.

Statistical Analysis

Data are presented as mean ± SD of at least three independent experiments. Comparisons were made using Student's t-test. Values of $P < 0.01$ were considered statistically significant.

Results

DSC

The acyl chains of phospholipids are subjected to phase transitions at specific temperatures, depending on the structure of the lipid. In details, lipids in hydrated membranes can be present in a gel phase (S) or in a liquid crystal phase (Lα), depending on the environmental temperature. The transition from the S to Lα phase occurs at the main phase transition temperature (Tm) which can be preceded by a pre-transition temperature (Tp), separating a lamellar gel (Lβ') from a ripple gel phase (Pβ'). The presence of the pre-transition mainly depends on the surface structure of the membrane [12]. Above the Tm, membrane changes to the liquid-disordered phase state and increases its permeability; this is due to the coexistence of membrane areas in both phases forming bound-areas with packing defect. This main transition is associated with gauche isomerizations of the acyl chains, which brings the bilayer from an ordered gel to a disordered fluid state. A similar fluidizing effect can be induced by the introduction of hydrophobic molecules within the ordered bilayer, causing then a decrease of Tm value and peak shape alteration [13].

The empty DPPC vesicles (DPPC-E) prepared and assayed at pH 7.4 presented a main transition peak at 42.14°C, whereas a shifted Tm (43.25°C) was recorded for pH 6.6 samples. Such temperature are greatly in agreement with what recently reported by Malekar et al., 2016 [14]. Additionally, the trend of Tm increasing with pH acidification, as consequence of hydration phenomena, was first reported for a wider pH range (pH 0-13) in 1987 [15]. The thermogram of DPPC-E at pH 6.6 was also displaying a pre-transition peak at 37.50 °C, which was not visible for the correspondent DPPC-E at pH 7.4. Both peaks had a Gaussian shape (Figure 1), even if at pH 7.4 the peak was wider and left-

skewed. The addition of F21 during vesicles formation resulted in the elimination of the pre-transition for pH 6.6 and in broaden endotherms for both pHs. As shown in Table 1, the Tm presented a shift to lower values when the vesicles were prepared in presence of F21. This shift was coherent with the drug/DPPC ratio, at both assayed pHs. The Tm shifts resulted statistically significant ($0.0005 < p < 0.003$) within each assayed pH for each drug/DPPC ratio. Additionally, the Tm values of pH6.6 vesicles were always significantly higher than those recorded for pH 7.4 vesicles, referring to similar drug/DPPC composition ($0.0001 < p < 0.0005$).

Despite the loss of the Gaussian shape, the enthalpy (ΔH) values of the main transition peaks for F21/DPPC vesicles were not statistically different from that obtained for plain DPPC samples. The only statistically significant different values ($p=0.0052$) were the ΔHs associated to the transitions of the plain vesicles (DPPC-E) at diverse pHs.

DLS

Plain DPPC (DPPC-E) and DPPC/F21 vesicles with the highest amount of drug (DPPC-X2) were characterized in terms of dimensional distribution by DLS analysis (Table 2). The addition of F21 to DPPC during DPPC-X2 vesicles formation determined the assembly of uniformly distributed vesicles with average diameter of 410.9 ± 15.7 nm and 361.8 ± 1.6 nm, in case of pH 6.6 and pH 7.4 respectively. However, the polydispersity at pH 6.6 was smaller, as confirmed by the calculated polydispersity index (PI), which resulted in 0.175 and 0.401 at pH 6.6 and 7.4, respectively. In absence of F21 (DPPC-E), the lipids did not assemble into submicron vesicles. Although the declared range of analysis for Coulter N4 PLUS is 3 nm - 3 μm, the instrument estimated the diameter distribution for DPPC-E samples. At both pH values, DPPC-E presented a poly-disperse population with an average diameter of 5-6 μm (5848.8 ± 145.2 nm at pH 6.6 and 5150.1 ± 130.7 nm at pH 7.4) and PI of 0.550-0.700, indicative for the presence of giant vesicles.

ATR/FTIR

The ATR/FT-IR spectra were used to assess the direct interaction between the bilayers and F21. The frequencies of the major functional groups were monitored in terms of shifts and comparative intensity changes, to be correlated with the interaction with the drug (Table 3). In particular, the following diagnostic signals were processed by means of second derivative spectrometry: CH_2 stretching of the lipid chains at 2915 cm^{-1} for asymmetric and 2849 cm^{-1} for symmetric, C=O stretching of the ester linkage at 1740 cm^{-1}, CH_2 scissoring at 1458 cm^{-1}, and P=O stretching at 1230 cm^{-1} (Figure 2). The $(CH_3)_3$-N^+ stretching signal of choline head at 925 cm^{-1} was not clearly detectable for any recorded spectra.

Starting from the signals related to the hydrocarbon chains, the asymmetric stretching was mainly affected by the interaction with F21. At both pHs, a statistically significant shift to higher wavenumbers was recorded, due to the interaction with F21 ($0.001 < p < 0.014$). Differently, the symmetric stretching was significantly affected only at pH 6.6 ($p=0.019$). These variations are commonly related to changes in vibrational and torsional motion of the phospholipids, due to an increase of gauche conformers in the aliphatic chains. Such conformational fluidization is ascribable to the interaction of the active compound with the lipid vesicles [16]. Concerning the splitting of the CH_2 scissoring signal due to acyl chain packing [17], it was clearly present only at pH 6.6, for both plain and F21/DPPC vesicles; at pH 7.4 the splitting was lost with the addition of F21 during vesicle formation (Figure 4, inserts).

Regarding the carbonyl stretching signal, the band results from the contributions of the carbonyl moieties of the two ester linkages to the glycerol backbone. In particular, the non-hydrogen-bonded *sn-1* C=O, located in the interior hydrophobic region, commonly results in higher frequency stretching bands, compared to the *sn-2* C=O involved in hydrogen-bonding and located closer to the polar head. The shape and the position of the C=O stretching signals changes accordingly with lipid assembly, hydration and presence of foreign compounds [18]. At both pHs, the *sn-1* and *sn-2* C=O signals were detected and a two-peak based deconvolution was performed in order to calculate their contribution to

the whole peak area. In both cases, the frequency and the relative area percentage varied with F21 addition to DPPC. Considering that the ATR/FT-IR measurements were performed on buffered hydrated lipid vesicles, the water molecules can be involved in hydrogen bonds with the carbonyl moieties of DPPC molecules. The signals recorded for DPPC-E at the two assayed pH, were correlated to a diverse hydration degree of the lipid vesicles: at pH 6.6 both carbonyl moieties had higher frequencies than the correspondent peaks of pH 7.4 sample, being thus more involved in hydrogen bonds with water. The increased hydration of pH 7.4 vesicles, was also reflected by the ν_{as} P=O band [19], falling at lower wavenumbers with respect to pH6.6 samples.

Second derivative Spectrophotometry

F21 partition in DPPC vesicles at pH 7.4 and pH 6.6 was estimated by means of second derivative spectrophotometry (Figure 3) [11]. The partition of F21 within DPPC vesicles determines a bathochromic shift of the main peaks of absorbance: from 260 to 270nm and from 319 to 324nm at both pHs, for plain F21 solution and F21/DPPC vesicles respectively (Figure 3). Additionally, two isosbestic points are present, at 236 and 290 nm.

The shift of the main peak of absorbance induces a variation of the second derivative intensities, mainly in the wavelength range 236-290nm, which is coherent with the amount of DPPC in the assayed specimen. The intensity variation (ΔD) at a predefined wavelength is necessary for the calculation of Kp (equation 3) and, even if the wavelength at which ΔD values are measured do not largely affect the calculated Kp, larger ΔD values allow for better precision [20]. For F21/DPPC samples, the larger intensity variations are obtained at 274nm and the estimated Kp and ΔDmax values are reported in Table 4. It appears that the partition coefficient is significantly higher at pH 7.4, resulting in a higher fraction of F21 in DPPC vesicles at this pH (Figure 4).

Discussion

The permeability across lipid membranes depends on the molecular structure of the permeant drug and on the phase state of the bilayer forming lipids. In case of inflammation and particularly in presence of solid tumors, the interstitial pHe shifts from physiological 7.4 to more acidic values. This acidosis plays a role in tumor development and progression as well as in tumor resistance to therapies, which is due not only to the peculiar profiles of stress-adapted cells, but also to the pH-induced alteration of the drug molecule in the extracellular environment. The investigated antitumor compound F21 presents a 2-indolecarboxylic acid with a predicted pK_a of 3.6 from the Human Metabolome Database [21-23] and a *N*-hydroxy moiety with pK_a of about 10, as estimated by Bykov *et al.* 2006 [24]. Thus, molecule F21 has a negative net charge at both investigated pHs, due to the presence of a dissociated carboxylic acid. From this viewpoint, the small pH variation under investigation is not supposed to affect the partitioning of F21 into the DPPC vesicles. However, the performed experimental studies showed a strong interaction between F21 and DPPC membranes at both assayed pHs, with a better partitioning at pH 7.4. Indeed, such behaviour was confirmed by all applied techniques and, as discussed below, it can be mainly related to the direct effect of pH variation on the lipid membrane assembly. Clearly, the slightly acidification of pH from 7.4 to 6.6 determined a better packing of the lipid and a reduced hydration of the vesicle surface resulting into a reduced partitioning of F21, with respect to pH 7.4.

DSC analyses evidenced a fluidization effect of F21 when interacting with the lipid bilayers, leading to a significant decrease of Tm values at both pHs, and the loss of the pre-transition peak for pH 6.6. The Tm shift occurring by drug addition was also associated to the loss of the Gaussian shape, especially for pH 6.6 samples, but without a significant alteration of the ΔH. Meanwhile, the higher Tm temperatures recorded for pH 6.6 samples as well as the presence of a pre-transition peak in DPPC-E pH 6.6 evidenced a stronger packing of the DPPC lipids at the more acidic pH. Such packing was also confirmed by the sharper shape and higher enthalpy of the Tm peak at this pH (6.6), indicating a stronger intermolecular interaction [25]. As a matter of fact, the observed deeper lipid packing can limit the access and reduce drug diffusion through the bilayer, thus correlating with the

lower membrane partitioning observed for F21 at pH 6.6 with respect to pH 7.4 (4 *vs* 8 $Kp/10^5$). Similarly, recent studies performed on DPPC bilayers and aimed at correlating the diffusion through membranes of anaesthetic drug molecules with protonation rate, reported a reduced drug diffusion through membranes having higher pre-transition enthalpy [26].

In line with these observations, the average mean diameters obtained by DLS measurements resulted slightly but significantly lower for DPPC-E pH 7.4 multilamellar vesicles, compared to that of pH 6.6 DPPC-E vesicles. Additionally, the interaction of F21 with DPPC lipids at both pHs determined a two orders reduction of the average mean diameter of the vesicles. This size variation is in agreement with previous literature correlating thermal stability with hydrodynamic radius, where increased membrane fluidity corresponds to vesicles size reduction [27].

The ATR/FT-IR analysis corroborated the previous observation highlighting different vibrational profiles of the carbonyl moieties belonging to the ester linkage region of DPPC-E, at the two-assayed pHs. The band positions and intensities suggested a higher hydration of the pH 7.4 bilayers, confirmed by the lower wavenumber of the phosphate band. The presence of F21 greatly disturbed both the ester linkage region and the aliphatic chain portion at both pHs. However, pH 6.6 samples still presented the splitting of the CH_2 scissoring band. Overall, the collected information suggested an interaction of F21 with the polar-middle portion of the lipid, including the glycerol backbone and the first part of methylene region, without a deeper insertion toward the end portion of the acyl chains. Clearly, the environmental acidification conditioned the arrangement of the lipids, leading to more packed and less hydrated vescicles at pH 6.6. Such interpretations are consistent with what reported by Claessens et al. 2004 [28], where the increased dehydration of lipid membranes corresponded to closer lipid packing, thicker membrane and higher rigidity. Despite the smaller pH gap assessed in the present paper, a similar behaviour is known for DPPC monolayers used as model for lung surfactant at air-water interfaces. Also in those models, pH changes determine the shift of the phase transition of DPPC, resulting in more expanded structures with a lower elasticity when pH changes

from acidic to basic values [29]. Indeed, the more rigid lipid assembly described for pH 6.6 bilayers renders the membranes less permeable to F21, resulting not only in a lower Kp but also in doped vesicles with residual rigidity. On the other hand, F21 interaction with DPPC at pH 7.4 appeared to be facilitated by the higher recorded hydration. In this case, F21 can participate to H-bond exchanges with water and DPPC, thus easing its partitioning within the bilayer to a more consistent lipid fluidization. The ATR/FT-IR analysis confirmed that the use of F21 implied a significant variation of the ν C=O but the position of ν_{as} P=O was not affected. Indeed, F21 can displace water molecules and interact through the N-OH group with the C=O moieties of the DPPC but the presence of a stable COO- charge on the drug molecule limits a direct interaction with the phosphate region of the lipids.

The results of the performed investigation highlight that F21 access to cell cytoplasm can easily occur through passive diffusion across cell membrane. However, the interstitial acidification would reduce F21 uptake, ending in an unfavourable partitioning effect. Consequently, the development of suitable prodrugs or F21 drug carriers is recommended for a faster translation to *N*-hydroxyindole based antitumor therapies. In this view, the performed investigation highlighted the interaction between F21 and PL, representing a solid starting point for the formulation of F21/liposomes. Accordingly, the observed pH effect appears useful for F21 leaking from liposomes in the tumor interstitial fluids, making the drug available for passive transport through cell membrane. Indeed, the investigated DPPC vesicles can be used as basis for the development of F21 carrying liposomes. The introduction of longer chain phospholipids such as distearoyl phosphatidylcholine (DSPC) as well as a balancing with cholesterol (Chol) units would contribute to vesicles stability upon storage and modulate drug release [30]. Concerning the preparation method to be applied for liposome formulation, it has been shown that F21 partitioning and interaction with the bilayers take advantages of the presence of superficial hydration. Hence, the use of methods not involving drying steps appears better suited. In particular, the use of reverse-phase evaporation method with basic pH buffered solutions is expected to positively contribute to F21 loading, in agreement to what ascertain in the reported study.

Considering F21 good solubility in ethanol and its high lipid interaction, ethanol injection, high-pressure homogenization as well as remote loading of pre-formed liposomes could be tested for larger scale production [31].

Conclusions

F21 greatly interacts with phospholipid membranes both at physiological and tumor interstitial acidic pH values, indicating a tendency to diffuse into PL membrane with a resulting fluidization effect. However, the small pH change from physiological pH 7.4 to tumor related acidic pH 6.6, significantly affected both F21-induced fluidization and F21 partitioning extent. Since F21 is carrying a negative net charge at both pH values, the lower interaction recorded at pH 6.6 was principally ascribable to a variation on lipid assembly. Mainly, the acidic environment had a dehydrating effect, primarily reflected on the phosphate and glycerol backbone regions, and which was responsible for a less accessible lipid structure. This aspect can be considered as a PL contribution to pH-dependent therapy-resistance, being not directly due to drug molecular features, but rather to a gained packing of the membranes at more acidic pH values. In case of *N*-hydroxyindole-2-carboxylic derivatives the development of suitable prodrugs as well as liposomal drug delivery system may overcome the observed limitations, further improving its antitumor efficacy.

As already stated, the present research evidenced significant changes of PL membrane properties directly due to F21 interactions. Recently, increasing evidence on the role of membrane lipids in the regulation of numerous cellular functions has been observed and membrane lipids have emerged as molecular target for antitumor drug candidates [32]. Being DPPC one of the most representative PL both in physiological and tumor tissues, further studies could be aimed at correlating the antitumor efficacy with the interaction of *N*-hydroxyindole-2-carboxylic derivatives with other lipid key-components of tumor cells.

Acknowledgments

The research project was supported by Progetti di ricerca di Ateneo PRA 2017 of the University of Pisa

References

1. Wojtkowiak JW, Verduzco D, Schramm KJ, Gillies RJ. Drug resistance and cellular adaptation to tumor acidic pH microenvironment. Molecular pharmaceutics. 2011;8(6):2032-8. doi:10.1021/mp200292c.
2. Kolosenko I, Avnet S, Baldini N, Viklund J, De Milito A. Therapeutic implications of tumor interstitial acidification. Seminars in cancer biology. 2017;43:119-33. doi:10.1016/j.semcancer.2017.01.008.
3. Bilge D, Sahin I, Kazanci N, Severcan F. Interactions of tamoxifen with distearoyl phosphatidylcholine multilamellar vesicles: FTIR and DSC studies. Spectrochimica acta Part A, Molecular and biomolecular spectroscopy. 2014;130:250-6. doi:10.1016/j.saa.2014.04.027.
4. Do TTT, Dao UPN, Bui HT, Nguyen TT. Effect of electrostatic interaction between fluoxetine and lipid membranes on the partitioning of fluoxetine investigated using second derivative spectrophotometry and FTIR. Chemistry and physics of lipids. 2017;207(Pt A):10-23. doi:10.1016/j.chemphyslip.2017.07.001.
5. Pignatello R, Musumeci T, Basile L, Carbone C, Puglisi G. Biomembrane models and drug-biomembrane interaction studies: Involvement in drug design and development. Journal of Pharmacy and Bioallied Sciences. 2011;3(1):4-14. doi:10.4103/0975-7406.76461.
6. Granchi C, Roy S, Giacomelli C, Macchia M, Tuccinardi T, Martinelli A et al. Discovery of N-hydroxyindole-based inhibitors of human lactate dehydrogenase isoform A (LDH-A) as starvation agents against cancer cells. Journal of medicinal chemistry. 2011;54(6):1599-612. doi:10.1021/jm101007q.
7. Granchi C, Calvaresi EC, Tuccinardi T, Paterni I, Macchia M, Martinelli A et al. Assessing the differential action on cancer cells of LDH-A inhibitors based on the N-hydroxyindole-2-carboxylate (NHI) and malonic (Mal) scaffolds. Organic & biomolecular chemistry. 2013;11(38):6588-96. doi:10.1039/c3ob40870a.
8. Maftouh M, Avan A, Sciarrillo R, Granchi C, Leon LG, Rani R et al. Synergistic interaction of novel lactate dehydrogenase inhibitors with gemcitabine against pancreatic cancer cells in hypoxia. British journal of cancer. 2014;110(1):172-82. doi:10.1038/bjc.2013.681.
9. Daniele S, Giacomelli C, Zappelli E, Granchi C, Trincavelli ML, Minutolo F et al. Lactate dehydrogenase-A inhibition induces human glioblastoma multiforme stem cell differentiation and death. Scientific reports. 2015;5:15556. doi:10.1038/srep15556.
10. Chetoni P, Monti D, Tampucci S, Matteoli B, Ceccherini-Nelli L, Subissi A et al. Liposomes as a potential ocular delivery system of distamycin A. International journal of pharmaceutics. 2015;492(1-2):120-6. doi:10.1016/j.ijpharm.2015.05.055.
11. Omran AA. An in vitro spectrometric method for determining the partition coefficients of non-steroidal anti-inflammatory drugs into human erythrocyte ghost membranes. Spectrochimica acta Part A, Molecular and biomolecular spectroscopy. 2013;104:461-7. doi:10.1016/j.saa.2012.12.002.
12. Hata T, Matsuki H, Kaneshina S. Effect of local anesthetics on the bilayer membrane of dipalmitoylphosphatidylcholine: interdigitation of lipid bilayer and vesicle-micelle transition. Biophysical Chemistry. 2000;87:25-36.
13. Riske KA, Barroso RP, Vequi-Suplicy CC, Germano R, Henriques VB, Lamy MT. Lipid bilayer pre-transition as the beginning of the melting process. Biochimica et Biophysica Acta (BBA) - Biomembranes. 2009;1788(5):954-63. doi:https://doi.org/10.1016/j.bbamem.2009.01.007.
14. Malekar SA, Sarode AL, BachII AC, Worthen DR. The localization of phenolic compounds in liposomal bilayers and their effects on surface characteristics and colloidal stability. AAPS PharmSciTech. 2016;17:1468-76.
15. Cevc G. How Membrane Chain Melting Properties Are Regulated by the Polar Surface of the Lipid Bilayer. Biochemistry. 1987;26:6305-10.

16. Mantsch HH, Chapman D, editors. Infrared Spectroscopy of Biomolecules. New York: Wiley-Liss; 1996.
17. Casal HL, Martin A, Mantsch HH. Infrared spectroscopic characterization of the interaction of lipid bilayers with phenol, salicylic acid and o-acetylsalicylic acid. Chemistry and physics of lipids. 1987;43:47-53.
18. Tsai YS, Ma SM, Nishimura S, Ueda I. Infrared spectra of phospholipid membranes: interfacial dehydration by volatile anesthetics and phase transition. Biochim Biophys Acta. 1990;1022(2):245-50. doi:10.1016/0005-2736(90)90120-d.
19. Cieślik-Boczula K, Maniewska J, Grynkiewicz G, Szeja W, Koll A, Hendrich AB. Interaction of quercetin, genistein and its derivatives with lipid bilayers – An ATR IR-spectroscopic study. Vibrational Spectroscopy. 2012;62:64-9. doi:10.1016/j.vibspec.2012.05.010.
20. Kitamura K, Goto T, Kitade T. Second derivative spectrophotometric-Kitamura. Talanta 46 (1998) 1433–1438. 1998;46:1433-8.
21. Wishart DS, Tzur D, Knox C, Eisner R, Guo AC, Young N et al. HMDB: the Human Metabolome Database. Nucleic acids research. 2007;35(Database issue):D521-6. doi:10.1093/nar/gkl923.
22. Wishart DS, Knox C, Guo AC, Eisner R, Young N, Gautam B et al. HMDB: a knowledgebase for the human metabolome. Nucleic acids research. 2009;37(Database issue):D603-10. doi:10.1093/nar/gkn810.
23. Wishart DS, Jewison T, Guo AC, Wilson M, Knox C, Liu Y et al. HMDB 3.0--The Human Metabolome Database in 2013. Nucleic acids research. 2013;41(Database issue):D801-7. doi:10.1093/nar/gks1065.
24. Bykov EE, Lavrenov SN, Preobrazhenskaya MN. Quantum-chemical investigation of the dependence of pKa on the calculated energy of proton removal for certain derivatives of indole and phenol. Chemistry of Heterocyclic Compounds. 2006;42(1):42-4. doi:10.1007/s10593-006-0044-z.
25. Smith EA, Dea PK. Differential Scanning Calorimetry Studies of Phospholipid Membranes: The Interdigitated Gel Phase. In: Elkordy AA, editor. Applications of Calorimetry in a Wide Context - Differential Scanning Calorimetry, Isothermal Titration Calorimetry and Microcalorimetry. Rijeka: InTech; 2013. p. Ch. 18.
26. Perez-Isidoro R, Sierra-Valdez FJ, Ruiz-Suarez JC. Anesthetic diffusion through lipid membranes depends on the protonation rate. Scientific reports. 2014;4:7534. doi:10.1038/srep07534.
27. Cinelli S, Onori G, Zuzzi S, Bordi F, Cametti C, Sennato S et al. Properties of mixed DOTAP-DPPC bilayer membranes as reported by differential scanning calorimetry and dynamic light scattering measurements. The journal of physical chemistry B. 2007;111(33):10032-9. doi:10.1021/jp071722g.
28. Claessens MM, van Oort BF, Leermakers FA, Hoekstra FA, Cohen Stuart MA. Charged lipid vesicles: effects of salts on bending rigidity, stability, and size. Biophysical journal. 2004;87(6):3882-93. doi:10.1529/biophysj.103.036772.
29. Lucero A, Rodríguez Niño M, Gunning A, Morris V, Wilde P, Rodríguez Patino J. Effect of Hydrocarbon Chain and pH on Structural and Topographical Characteristics of Phospholipid Monolayers. J Phys Chem B 2. 2008;112:7651-61.
30. Briuglia ML, Rotella C, McFarlane A, Lamprou DA. Influence of cholesterol on liposome stability and on in vitro drug release. Release Drug Deliv. and Transl. Res. 2015, 5: 231
31. Kraft JC, Freeling JP, Wang Z, Ho RJY. Emerging Research and Clinical Development Trends of Liposome and Lipid Nanoparticle Drug Delivery Systems. Journal of Pharmaceutical Sciences, 2014, 103 (1): 29-52
32. Tan LT-H, Chan K-G, Pusparajah P, et al. Targeting Membrane Lipid a Potential Cancer Cure? Frontiers in Pharmacology. 2017;8:12.

TABLES

Table 1. Transition temperature and enthalpy variations recorded by DSC measurements. Each reported value is the average of three independent measurements.

pH	Vesicles	DPPC/F21	Tm (°C)	ΔH (J/g)
7.4	DPPC-E	-	42.14 ± 0.10	0.93 ± 0.15
7.4	DPPC-X1	1 : 0.06	41.42 ± 0.04	0.89 ± 0.12
7.4	DPPC-X2	1 : 0.13	39.07 ± 0.51	1.15 ± 0.41
6.6	DPPC-E	-	43.25 ± 0.06	1.48 ± 0.08
6.6	DPPC-X1	1 : 0.06	41.81 ± 0.06	1.35 ± 0.08
6.6	DPPC-X2	1 : 0.13	40.73 ± 0.02	1.13 ± 0.30

Table 2. DLS Diameter distribution recorded for plain and F21

			Diameter Distribution	
pH	**Vesicles**	**DPPC/F21**	**Unimodal Intensity Distribution**	
			(nm ± SD)	**PI**
7.4	DPPC-E	-	5150.1 ± 130.7	0.718
7.4	DPPC-X2	1 : 0.13	361.8 ± 1.6	0.401
6.6	DPPC-E	-	5848.8 ± 145.2	0.556
6.6	DPPC-X2	1 : 0.13	410.9 ± 15.7	0.175

Table 3: Main frequencies of lipid vesicles at pH 7.4 and 6.6 and in presence of F21

Sample	pH	ν_{as} C-H	ν_s C-H	δ CH_2	ν_s[a] C=O sn1	ν_s[a] C=O sn2	ν_{as} P=O
DPPC-E	7.4	2916.6±0.9	2849.3±1.4	1458.9±2.4	1737.2 (85)	1718.2 (15)	1227.4±0.9
DPPC-X2	7.4	2918.5±1.2	2850.3±0.1	1465.1±1.8	1739.5 (70)	1721.5 (30)	1227.4±1.0
DPPC-E	6.6	2917.0±1.1	2849.1±1.1	1456.5±1.8	1739.6 (61)	1721.3 (40)	1234.2±1.4
DPPC-X2	6.6	2920.1±0.8	2849.1±1.1	1458.2±2.5	1737.7 (50)	1724.3 (50)	1234.2±2.1

[a]Peak wavenumber values obtained by performing the signal deconvolution. The subcomponent peak area (%) is reported in brackets

Table 4: Partition coefficients of F21 in DPPC vesicles at pH7.4 and pH6.6, and relevant ΔDmax from second derivative spectra.

pH	$Kp/10^5$	$\Delta Dmax/10^4$
7.4	8.03±0.63	5.65±0.22
6.6	3.815±0.32	6.39±0.45

Caption to Figures:

Structure 1: Chemical structure of the antitumor agent F21

Figure 1: DSC heating thermograms of F21/DPPC membranes at pH 6.6 and pH 7.4. For clarity, thermograms are offset vertically

Figure 2: ATR/FT-IR spectra of DPPC-E (Blue) and DPPC-X2 (Red) suspensions at pH 6.6 (dashed lines) and pH 7.4 (full lines). The insert displays the second derivative of the CH_2 scissoring region: overlaying of DPPC-E (Blue) and DPPC-X2 (Red) spectra at pH 7.4 and 6.6, respectively

Figure 3: Second derivative spectra of the absorption spectra of F21 in presence of various concentrations (mM) of DPPC vesicles at the two different pHs: (1) 0; (2) 0.034; (3) 0.102; (4) 0.136; (5) 0.204; (6) 0.306; (7) 0.510; (8) 0.816.

Figure 4: Fraction of F21 in DPPC vesicles at various DPPC concentrations at pH7.4 (∗) and pH6.6 (O).

Structure 1

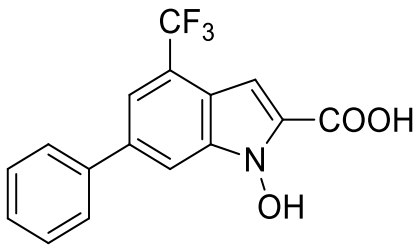

Figure 1

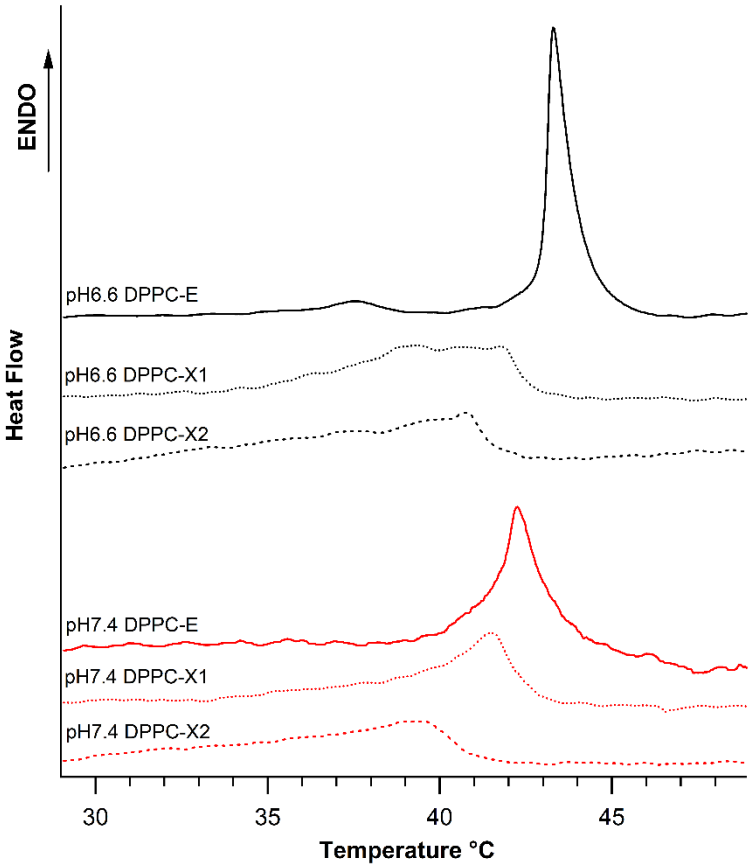
ENDO
Heat Flow
pH6.6 DPPC-E
pH6.6 DPPC-X1
pH6.6 DPPC-X2
pH7.4 DPPC-E
pH7.4 DPPC-X1
pH7.4 DPPC-X2
30
35
40
45
Temperature °C

.

Figure 2

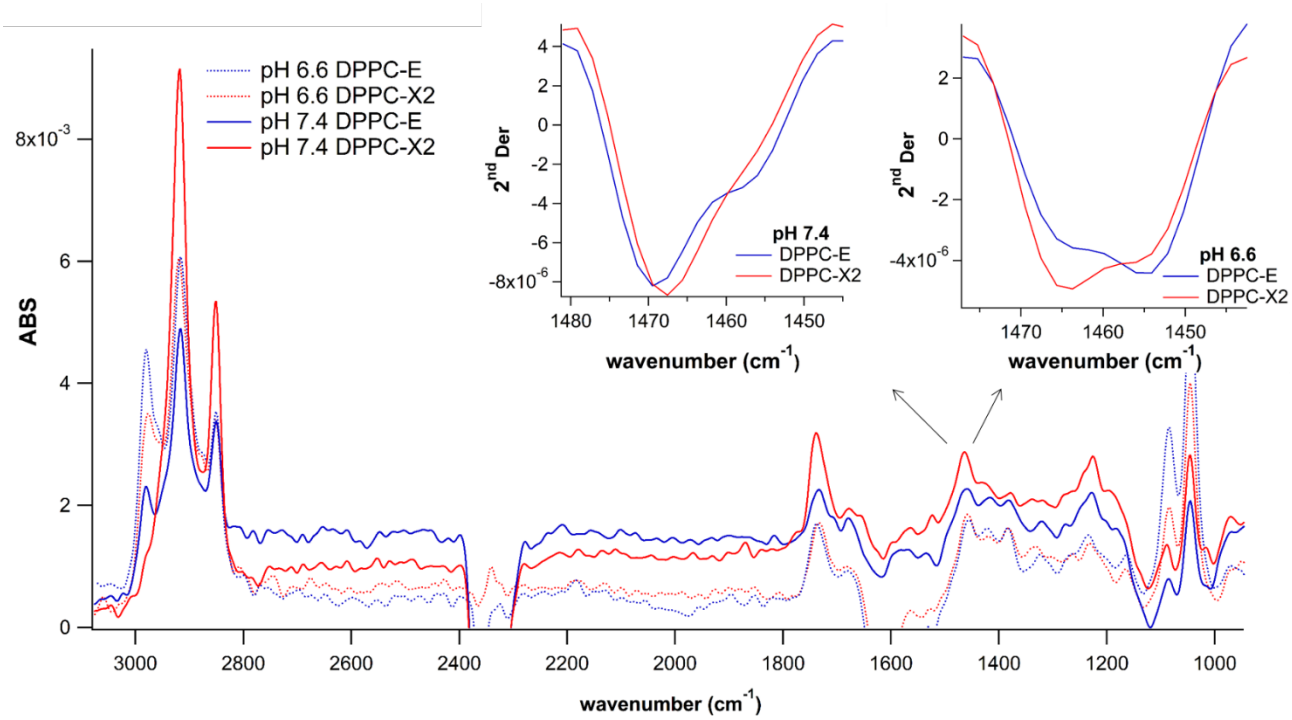
pH 6.6 DPPC-E
pH 6.6 DPPC-X2
pH 7.4 DPPC-E
pH 7.4 DPPC-X2
ABS
8x10-3
6
4
2
0
3000
2800
2600
2400
2200
2000
1800
1600
1400
1200
1000
wavenumber (cm-1)
2nd Der
4
2
0
-2
-4
-6
-8x10-6
1480
1470
1460
1450
pH 7.4
DPPC-E
DPPC-X2
wavenumber (cm-1)
2nd Der
2
0
-2
-4x10-6
1470
1460
1450
pH 6.6
DPPC-E
DPPC-X2
wavenumber (cm-1)

.

Figure 3

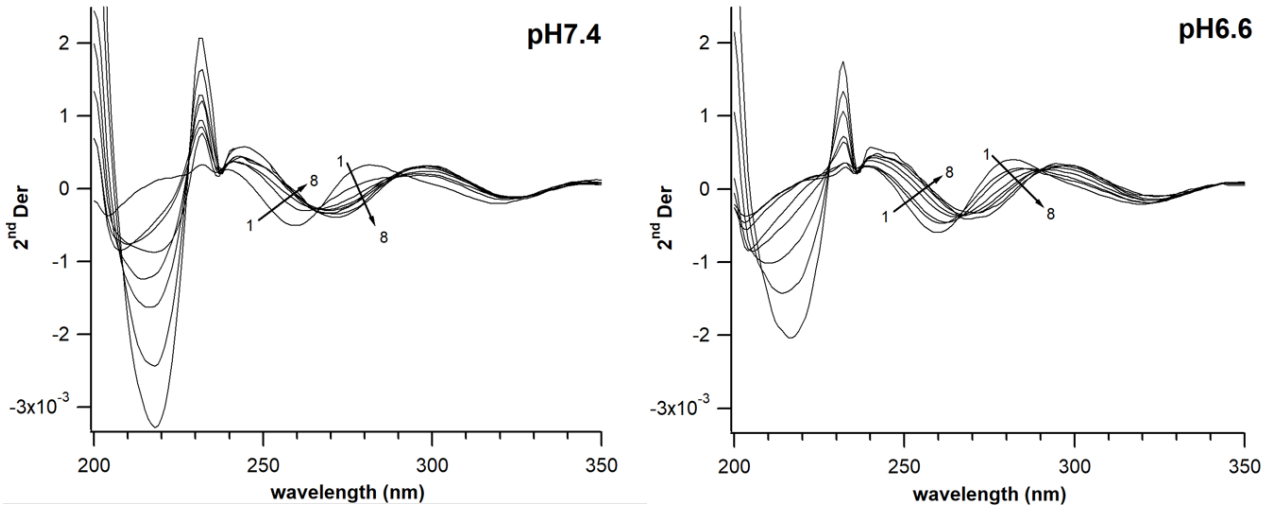
pH7.4
pH6.6
2nd Der
wavelength (nm)
2
1
0
-1
-2
-3x10-3
200
250
300
350
1
8

Figure 4